

Supporting Information

Novel and Dual-Mode Strain-Detecting Performance Based on Layered NiO/ZnO P-N Junction for Flexible Electronics

*Minxuan Xu, Xin Li, Chengchao Jin, Zhiwei He, Xuefeng Zhang, Qi Zhang**

School of Materials and Environmental Engineering, Hangzhou Dianzi University, Hangzhou
310018, China

*Corresponding authors, E-mail: qizhang@hust.edu.cn

Table of contents

- 1. Material and Methods**
- 2. Supplementary Tables and Figures**
- 3. Mechanism Analysis**
- 4. Supplementary Videos**
- 5. Supplementary References**

1. Materials and Methods

Material: The CH₃CH₂OH (99.7 %) was purchased from Sinopharm Chemical Reagent Co., Ltd. Ar and N₂ gas were provided by Huanyu Jinghui Jingcheng Gas Technology Co., Ltd., Beijing. The conductive PET (100 μm thickness, 95 % transparency and 10⁴~10⁵ Ω) was supplied by Xinhe Yuantu Electronic Packaging Material Co., Ltd., Shenzhen. 4N-purity ZnO and NiO targets were offered by Zhongnuo New Material Technology Co., Ltd., Beijing.

Preparation of flexible DMPT: A commercial PET substrate with ITO film grown on top was chosen as a flexible substrate. It was treated with alcohol, deionized water and dried by N₂ to remove surface contaminants. An 80 nm thick p-type NiO layer was grown on the PET substrate *via* RF magnetron sputtering at 30 sccm Ar flow rate, 1.2 Pa chamber pressure and 100 W sputtering power, respectively. Then, the chamber pressure and sputtering power were adjusted to 1.0 Pa and 80 W to obtain a 320 nm thick n-type ZnO layer on the top of the NiO film. It was properly masked to cover only part of the PET substrate before the first sputtering. After all sputtering was completed, the masks were removed and the Ag electrodes were fabricated on the exposed ITO and ZnO, respectively. The flexible DMPT is assembled without further encapsulation.

Characterization and measurement: The as-fabricated DMPT is connected with the fixtures of the characterization and measurement system through the conductive tapes. The Photoluminescence spectra was recorded by the Raman spectroscopy (Horiba, JY-HR800) installed with a He-Cd laser ($\lambda=325$ nm). The morphology and layer thickness of NiO and ZnO film were observed by a scanning electron microscope (JEOL, JSM-6490). An X-ray diffractometer (Rigaku, DMAX-RB) was used to measure the crystallinity of the sputtered films. The electromechanical properties of the fabricated sensors were investigated by the semiconductor characterization system (Keithley, 4200-SCS). All measurements were performed at room temperature.

2. Supplementary Tables and Figures

2.1 Tables

Table S1. The longevity comparison of recent reported strain sensors (The “-” means Not Available)

Mechanism	Material	Durability	Self-power	Static strain	Reference
Piezoelectric	BaTiO ₃ /Bacterial cellulose	3000	✓	-	[1] <i>Adv. Sci.</i> 2016 , 3, 1500257
	PTO NT array	4500	✓	-	[2] <i>Adv. Mater.</i> 2017 , 29, 1604500
	PbI ₂ nanosheets	4500	✓	-	[3] <i>Nano Energy</i> 2018 , 49, 7
	h-BN nanoflakes	5000	✓	-	[4] <i>ACS Appl. Mater. Inter.</i> 2019 , 11, 37920
	Kirigami-based piezoelectric systems	1500	✓	-	[5] <i>Adv. Mater. Technol.</i> 2019 , 4, 1900100
Piezoresistive	Graphene/PI	2000	-	✓	[6] <i>ACS Nano</i> 2015 , 9, 8933
	MoS ₂ /Graphene film	1000	-	✓	[7] <i>Adv. Mater.</i> 2016 , 28, 2556
	Graphene/TPU	50	-	✓	[8] <i>J. Mater. Chem. C</i> 2017 , 5, 73
	Ag NWs/TPU/PDMS	1600	-	✓	[9] <i>J. Mater. Chem. C</i> 2017 , 5, 7035
	PS/Ag/PDMS	30	-	✓	[10] <i>Nano Res.</i> 2018 , 11, 1938
Piezoelectric Band theory	NiO/ZnO p-n junction	2000	✓	✓	This work

Table S2. The performance comparison of recent reported flexible strain sensors (The “-” means Not Available).

Mechanism	Material	Stretch ability	Sensitivity or GF		Reference
			dynamic strain	static strain	
Piezoelectric	CNT/PTFE/fiber	25%	1.9 nA·% ⁻¹	-	[11] <i>Adv. Funct. Mater.</i> 2015
	Ionic polymer membrane	1.8%	3 mV·% ⁻¹	-	[12] <i>Small</i> , 2016
	PTO NT array	1.8%	1.7 nA·% ⁻¹	-	[2] <i>Adv. Mater.</i> 2017
	PbI ₂ nanosheets	0.34%	9.8 nA·% ⁻¹	-	[3] <i>Nano Energy</i> 2018
	α-In ₂ Se ₃ /PET	0.76%	5.2 nA·% ⁻¹	-	[13] <i>ACS Nano</i> 2018
	Kirigami-based piezoelectric systems	30%	4 nA·% ⁻¹	-	[5] <i>Adv. Mater. Technol.</i> 2019
Piezoresistive	ITO nanocrystal films	0.6%	-	23	[14] <i>Nanoscale</i> 2015
	Ag NWs/PDMS	35%	-	20	[15] <i>Nano Lett.</i> 2015
	MoS ₂ /Graphene	5%	-	50	[7] <i>Adv. Mater.</i> 2016
	WS ₂ films/PET	1%	-	14	[16] <i>Mater. Lett.</i> 2017
	Au NPs/paper	0.6%	-	75.8	[17] <i>ACS Appl. Mater. Inter.</i> 2017
	CT/PDMS	10%	-	18.5	[18] <i>Sci. Rep.</i> 2017
	Carbonized crepe paper	6%	-	10.1	[19] <i>Adv. Funct. Mater.</i> 2018
	RGO/GF/silicone	4%	-	13.1	[20] <i>ACS Appl. Mater. Inter.</i> 2018
ReS ₂ flake/PI	0.14%	-	60.5	[21] <i>ACS Nano</i> 2019	
Piezoelectric Band theory	NiO/ZnO p-n junction	1%	7.67 nA·%⁻¹	196	This work

2.2 Figures

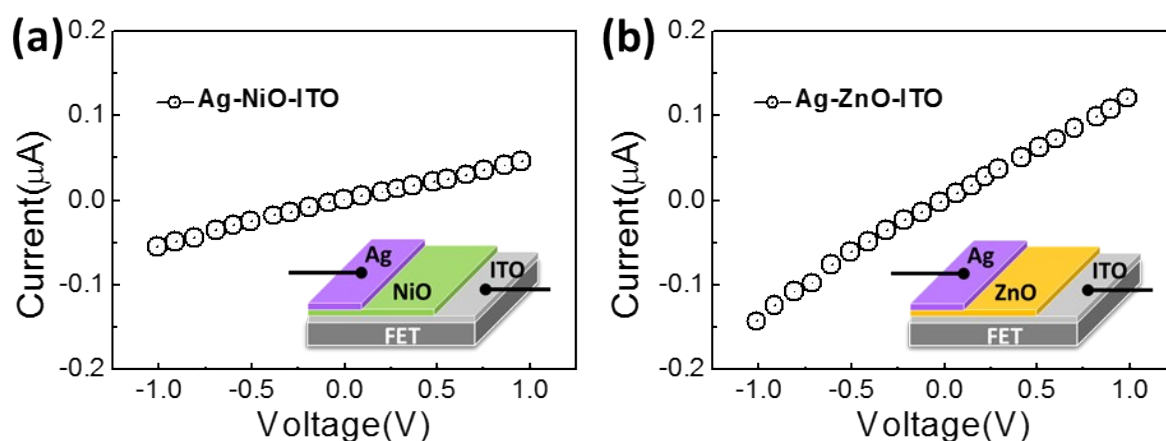


Figure S1. The I-V curves of the semiconductor and electrodes: (a) As-fabricated device with structure of Ag-NiO (80 nm)-ITO, (b) As-fabricated device with structure of Ag-ZnO (320 nm)-ITO. The insets are the schematic diagrams.

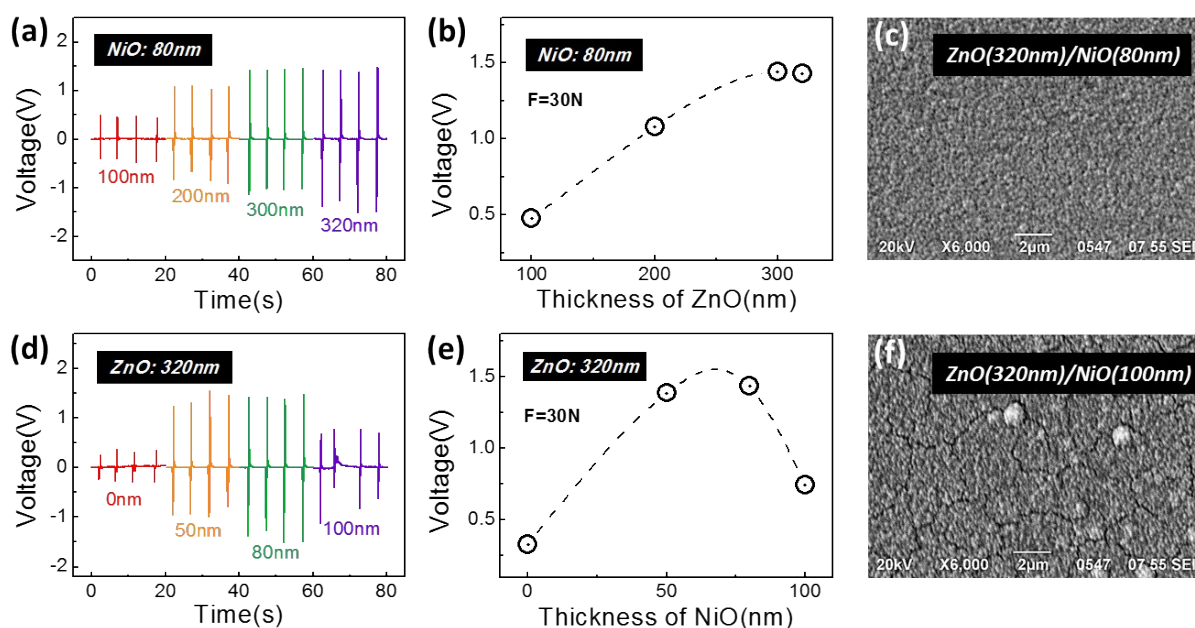


Figure S2. Output performance of the DMPT based on ZnO/NiO junction with different thickness ratio: (a) Output voltage of devices with different ZnO thickness, (b) The relationship between ZnO thickness and output voltage, (c) The top view SEM of ZnO(320nm)/NiO(80nm), (d) Output voltage of sensors with different NiO thickness, (e) The relationship between NiO thickness and output voltage, (f) The top view SEM of ZnO(320nm)/NiO(100nm).

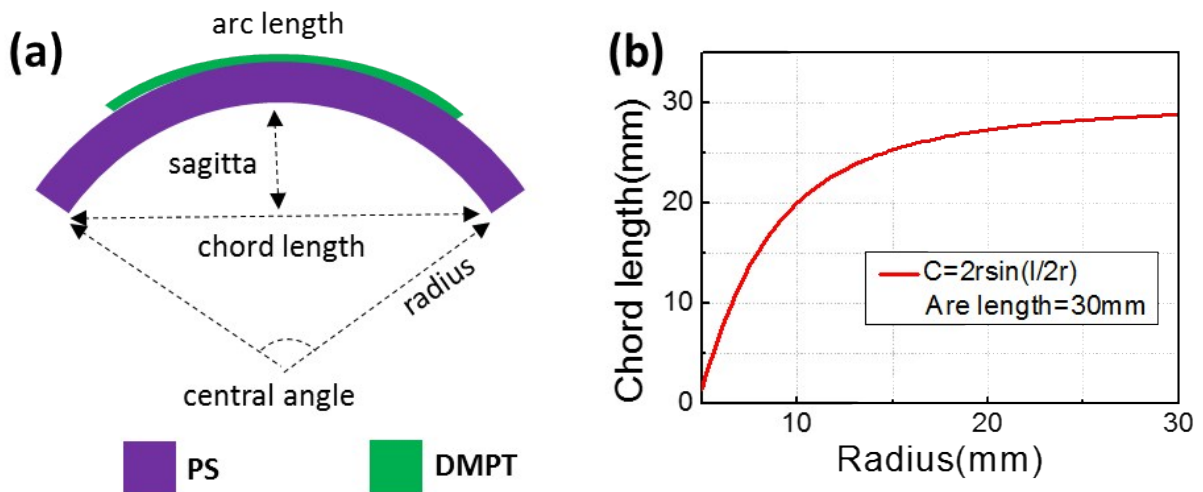


Figure S3. Method of calculating the effective strain during the DMPT/PS bending process: (a) Schematic model diagram of a bending sensor with physical parameters, (b) The chord length as a function of radius at a fixed arc length of 30 mm.

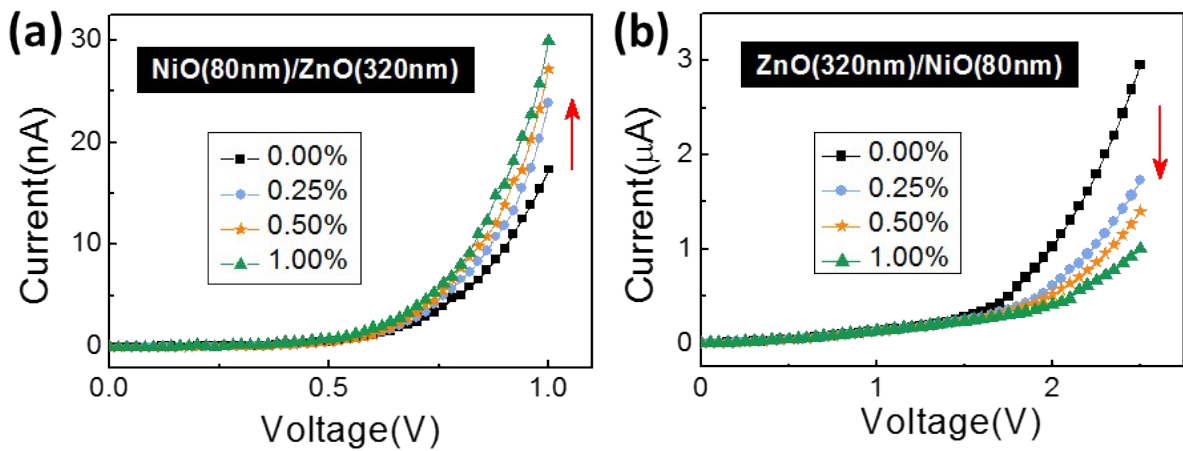


Figure S4. I-V curves of DMPT based on different structure under horizontal tensile strain: (a) As-fabricated Ag-NiO-ZnO-ITO-Ag, (b) As-fabricated Ag-ZnO-NiO-ITO-Ag.

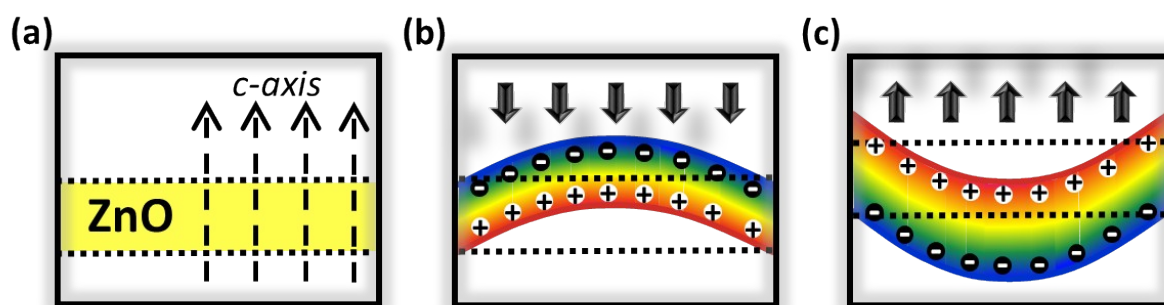


Figure S5. Piezoelectric potential generated by ZnO layer during the DMPT/PS bending process: (a) Unstrained state, (b) Under horizontal stretched state, (c) Under horizontal compressed state.

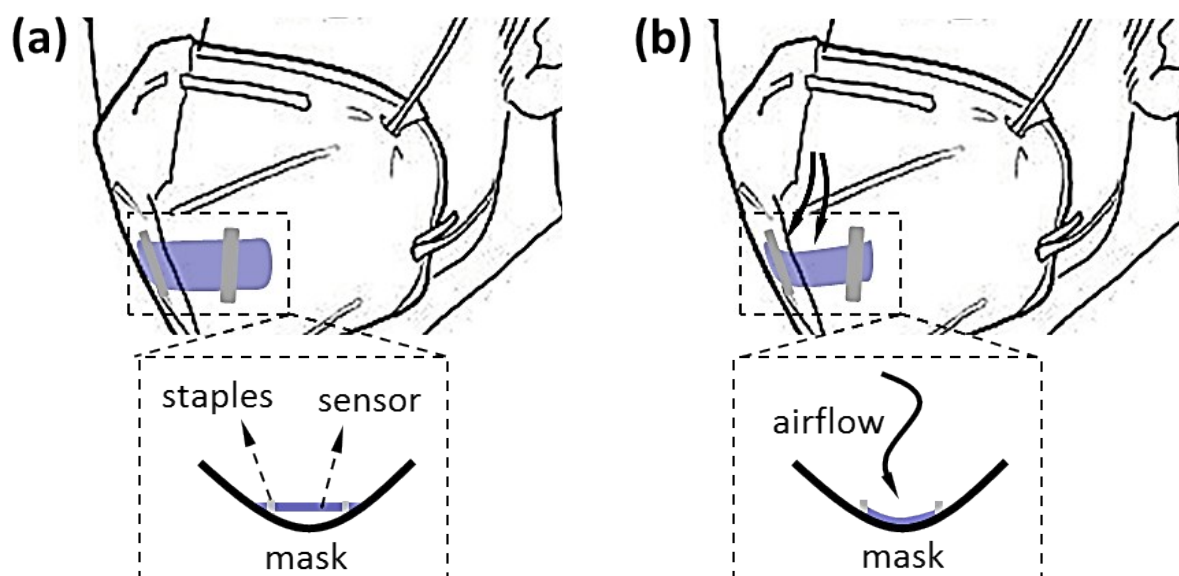


Figure S6. Schematic diagram of DMPT mounted on the inside of the mask: (a) Without the exhaled airflow acts on the surface of the device, (b) With the exhaled airflow acts on the surface of the device. The dotted frame is the corresponding top view.

3. Mechanism Analysis

3.1 Method of calculating the effective strain

According to Figure S3a, the DMPT/PS is bent with radius r , chord length c , central angle θ and arc length l . The relationships between the physical parameters can be expressed as:

$$\theta = \frac{l}{r} \quad (\text{S1})$$

$$\sin\left(\frac{\theta}{2}\right) = \frac{c}{2r} \quad (\text{S2})$$

After substituting equation S1 into S2, we obtain the chord length c as a function of radius r (Figure S3b):

$$c = 2r \cdot \sin\left(\frac{l}{2r}\right) \quad (\text{S3})$$

The effective tensile strain of the device is defined as ε , which can be represented by [22]:

$$\varepsilon = \frac{\Delta l}{l} = \frac{\theta_2 \cdot (r_2 - z) - \theta_1 \cdot (r_1 - z)}{\theta_1 \cdot (r_1 - z)} \quad (\text{S4})$$

Where z is the distance away from neutral layer of PS, r_1 and r_2 are the relevant radius at bending central angle θ_1 and θ_2 , respectively. Because r_1 is far greater than z , and $\theta_1 \cdot r_1 \approx \theta_2 \cdot r_2$, the equation S4 is equal to:

$$\varepsilon = \frac{z \cdot (\theta_1 - \theta_2)}{\theta_1 \cdot r_1} = z \cdot \left(\frac{1}{r_1} - \frac{1}{r_2} \right) \quad (\text{S5})$$

As the original state of the PS substrate is flat, the r_1 tends to infinity. Finally, the effective tensile strain can be calculated as follow [23, 24]:

$$\varepsilon = \frac{-z}{r_2} = \frac{-h}{2r} \quad (\text{S6})$$

Where h is the thickness of PS. In the same way, the effective compressive strain is given analytically as:

$$\varepsilon = \frac{h}{2r} \quad (\text{S7})$$

3.2 Gauge factor of the static strain

The current variation ratios ($\Delta I/I_0$) was chosen to express the change of electrical property in the process of strain applied, which can be calculated as follow [25]:

$$\frac{\Delta I}{I_0} = \frac{I_n - I_0}{I_0} \quad (\text{S8})$$

Where I_0 is the initial current, I_n is the response current at a strain ε .

Gauge factor (GF), the change of electrical property when the strain change $d\varepsilon$, is employed to quantitatively express the sensitivity of strain sensors based on piezoresistive effect [26]. In this work, the increment of electrical property is defined as $d(\Delta I/I_0)$, so GF is expressed as:

$$GF = \frac{d(\Delta I/I_0)}{d\varepsilon} \approx \frac{\delta(\Delta I/I_0)}{\delta\varepsilon} \quad (S9)$$

As the strain increases, the $\Delta I/I_0$ curve shows a linear increasing (Figure 3e, $R^2=0.963$) or decreasing (Figure 3b, $R^2=0.884$). The $\delta(\Delta I/I_0)$ can be replaced by $\Delta(\Delta I/I_0)$ if the $\Delta\varepsilon$ is small enough, that is, the value of GF is equal to the slope of $\Delta I/I_0$ - ε curve [27].

3.3 Sensitivity of the dynamic strain

In dynamic strain mode, the initial current I_0 is 0 when no strain is applied, which will make formula S8 meaningless. Therefore, the expression S9 of GF under static strain is not applicable in dynamic strain detection. To demonstrate the output of current pulse as a function of applied dynamic strain, the sensitivity (S) of sensors based on piezoelectric effect is generally defined as [28]:

$$S = \frac{dI}{d\varepsilon} \approx \frac{\delta I}{\delta\varepsilon} = \frac{I_n - I_0}{\varepsilon_n - \varepsilon_0} \quad (S10)$$

Where I_0 and ε_0 are the initial current and strain, I_n is the response current at a strain ε_n . Therefore, the value of S is equal to the slope of I - ε curve.

4. Supplementary Videos

Video-1: The real-time output current of the DMPT with dynamic tensile strain without bias voltage.

Video-2: The real-time output current of the DMPT with dynamic compressive strain without bias voltage.

Video-3: The current response of the DMPT with static compressive strain with a bias of 1V.

5. Supplementary References

- [1]. G. J. Zhang, Q. L. Liao, Z. Zhang, Q. J. Liang, Y. L. Zhao, X. Zheng, Y. Zhang, *Adv. Sci.*, 2016, **3**, 1500257.
- [2]. Y. B. Lee, J. K. Han, S. Noothongkaew, S. K. Kim, W. Song, S. Myung, S. S. Lee, J. Lim, S. D. Bu, K-S. An, *Adv. Mater.*, 2017, **29**, 1604500.
- [3]. H. B. Song, I. Karakurtb, M. S. Wei, N. Liu, Y. Chu, J. W. Zhong, L. W. Lin, *Nano Energy*, 2018, **49**, 7-13.
- [4]. G-Ja. Lee, M-K. Lee, J-J. Park, D. Y. Hyeon, C. K. Jeong, K-il. Park, *ACS Appl. Mater. Interfaces*, 2019, **11**, 37920-37926.
- [5]. R. J. Sun, S. C. Carreira, Y. Chen, C. Q. Xiang, L. L. Xu, B. Zhang, M. D. Chen, I. Farrow, F. Scarpa, J. Rossiter, *Adv. Mater. Technol.*, 2019, **4**, 1900100.
- [6]. Y. Y. Qin, Q. Y. Peng, Y. J. Ding, Z. S. Lin, C. H. Wang, Y. Li, F. Xu, J. J. Li, Y. Yuan, X. D. He, Y. B. Li, *ACS Nano*, 2015, **9**, 8933-8941.
- [7]. M. Park, Y. J. Park, X. Chen, Y-K. Park, M-S. Kim, J-H. Ahn, *Adv. Mater.*, 2016, **28**, 2556-2562.
- [8]. H. Liu, M. Y. Dong, W. J. Huang, J. C. Gao, K. Dai, J. Guo, G. Q. Zheng, C. T. Liu, C. Y. Shen, Z. H. Guo, *J. Mater. Chem. C*, 2017, **5**, 73-83.
- [9]. L. J. Lu, X. D. Wei, Y. Zhang, G. Q. Zheng, K. Dai, C. T. Liu, C. Y. Shen, *J. Mater. Chem. C*, 2017, **5**, 7035-7042.
- [10]. Y. G. Hu, T. Zhao, P. L. Zhu, Y. Zhang, X. W. Liang, R. Sun, C. P. Wong, *Nano Res.*, 2018, **11**, 1938-1955.
- [11]. J. W. Zhong, Q. Z. Zhong, Q. Y. Hu, N. Wu, W. B. Li, B. Wang, B. Hu, J. Zhou, *Adv. Funct. Mater.*, 2015, **25**, 1798-1803.
- [12]. Y. Liu, Y. Hu, J. J. Zhao, G. Wu, X. M. Tao, W. Chen, *Small*, 2016, **12**, 5074-5080.
- [13]. F. Xue, J. W. Zhang, W. J. Hu, W-T. Hsu, A. Han, S-F. Leung, J-K. Huang, Y. Wan, S. H. Liu, J. L. Zhang, J-H. He, W-H. Chang, Z. L. Wang, X. X. Zhang, L-J. Li, *ACS Nano*, 2018, **12**, 4976-4983.

- [14]. N. M. Sangeetha, M. Gauvin, N. Decorde, F. Delpech, P. F. Fazzini, B. Viallet, G. Viau, J. Grisolia, L. Ressler, *Nanoscale*, 2015, **7**, 12631-12640.
- [15]. K. K. Kim, S. Hong, H. M. Cho, J. Lee, Y. D. Suh, J. Ham S. H. Ko, *Nano Lett.*, 2015, **15**, 5240-5247.
- [16]. H-Y. Qi, W-T. Mi, H-M. Zhao, T. Xue, Y. Yang, T-L. Ren, *Mater. Lett.*, 2017, **201**, 161-164.
- [17]. X. Q. Liao, Z. Zhang, Q. J. Liang, Q. L. Liao, Y. Zhang, *ACS Appl. Mater. Interfaces*, 2017, **9**, 4151-4158.
- [18]. Y-Q. Li, P. Huang, W-B. Zhu, S-Y. Fu, N. Hu, K. Liao, *Sci. Rep.*, 2017, **7**, 45013.
- [19]. S. Chen, Y. J. Song, D. Y. Ding, Z. Ling, F. Xu, *Adv. Funct. Mater.*, 2018, **28**, 1802547.
- [20]. Y. F. Fu, Y. Q. Li, Y. F. Liu, P. Huang, N. Hu, S-Y. Fu, *ACS Appl. Mater. Interfaces*, 2018, **10**, 35503-35509.
- [21]. C. H. An, Z. H. Xu, W. F. Shen, R. J. Zhang, Z. Y. Sun, S. J. Tang, Y-F. Xiao, D. H. Zhang, D. Sun, X. D. Hu, C. G. Hu, L. Yang, J. Liu, *ACS Nano*, 2019, **13**, 3310-3319.
- [22]. X. Q. Liao, Q. L. Liao, X. Q. Yan, Q. J. Liang, H. N. Si, M. H. Li, H. L. Wu, S. Y. Cao, Y. Zhang, *Adv. Funct. Mater.*, 2015, **25**, 2395-2401.
- [23]. S. Lee, A. Reuveny, J. Reeder, S. Lee, H. Jin, Q. Liu, T. Yokota, T. Sekitani, T. Isoyama, Y. Abe, Z. G. Suo, T. Someya, *Nat. Nanotechnol.*, 2016, **11**, 472-479.
- [24]. C. R. P. Inbaraj, R. J. Mathew, G. Haider, T-P. Chen, R. K. Ulaganathan, R. Sankar, K. P. Bera, Y-M. Liao, M. Kataria, H-I. Lin, F. C. Chou, Y-T. Chen, C-H. Lee, Y-F. Chen, *Nanoscale*, 2018, **10**, 18642-18650.
- [25]. W. Feng, W. Zheng, F. Gao, X. S. Chen, G. B. Liu, T. Hasan, W. W. Cao, P. A. H, *Chem. Mater.*, 2016, **28**, 4278-4283.
- [26]. X. M. Li, T. T. Yang, Y. Yang, J. Zhu, L. Li, F. E. Alam, X. Li, K. L. Wang, H. Y. Cheng, C-T. Lin, Y. Fang, H. W. Zhu, *Adv. Funct. Mater.*, 2016, **26**, 1322-1329.
- [27]. X. Y. Meng, S. F. Zhao, Z. Zhang, R. L. Zhang, J. H. Li, J. F. Leng, D. X. Cao, G. P. Zhang, R. Sun, *J. Mater. Chem. C*, 2019, **7**, 7061-7072.
- [28]. S. Wagner, C. Y. Yim, N. McEvoy, S. Kataria, V. Yokaribas, A. Kuc, S. Pindl, C-P. Fritzen, T. Heine, G. S. Duesberg, M. C. Lemme, *Nano Lett.*, 2018, **6**, 3738-3745.